Fluid Structure Interaction of Parachutes in Supersonic Planetary Entry

Anita Sengupta*
Jet Propulsion Laboratory, California Institute of Technology, Pasadena, CA, 91109

A research program to provide physical insight into disk-gap-band parachute operation in the supersonic regime on Mars was conducted. The program included supersonic wind tunnel tests, computational fluid dynamics and fluid structure interaction simulations. Specifically, the nature and cause of the "area oscillation" phenomenon were investigated to determine the scale, aerodynamic, and aero-elastic dependence of the supersonic parachute collapse and re-inflation event. A variety of non-intrusive, temporally resolved, and high resolution diagnostic techniques were used to interrogate the flow and generate validation datasets. The results of flow visualization, particle image velocimetry, load measurements, and photogrammetric reconstruction will be presented. Implications to parachute design, use, and verification will also be discussed.

Nomenclature

D_o	=	Parachute nominal diameter
d	=	Command module maximum diameter
x/d	=	Non-dimensional trailing distance
C_D	=	Drag coefficient
Q	=	Dynamic Pressure
Re	=	Reynolds number
α	=	Angle of attack
T_{inf}	=	Free stream temperature
ρ	=	Density
μ	=	Viscosity
T_{inf}	=	Free stream temperature
S_o	=	Parachute nominal area
t_i	=	Inflation time

I. Introduction

The aerodynamic decelerator is a critical element of Entry, Descent, and Landing (EDL) aerospace systems. The most common implementation of an aerodynamic decelerator, in both Earth and extraterrestrial applications, is the parachute. A parachute is a drag device constructed from high strength-to-weight textile materials with application in the subsonic to supersonic regime. Parachutes are typically used to decelerate the payload to low subsonic speeds enabling separation of vehicle stages, initiation of retro-propulsive terminal descent, or to provide a safe terminal velocity for landing. These functions can be accomplished with a single parachute or multi-chute systems according to the mission architecture.

Parachutes are regularly used in the subsonic regime for sport and military parachuting, aerial delivery, aircraft escape, military recovery systems, cargo drops, aircraft landing deceleration, and Earth re-entry systems. The supersonic use of parachutes has been limited, however, due to performance, stability, and structural concerns associated with this regime[1,2]. Supersonic uses of parachutes include missile recovery, Mars entry-systems, and ballistic nose cone recovery [3]. A known instability exists for operation above Mach 1.5, a result of the fluid-structure-interaction between the flow-field and canopy fabric [4,5]. The supersonic instability has perplexed the decelerator community for the past several decades. It is only recently that this mystery has been solved, in support of near-term missions to Mars that have payload requirements which necessitate application of large-scale

* Senior Engineer, Systems Engineering, MS-301-365, Senior Member.

supersonic aerodynamic decelerators. Recent experimental and analytical work with subscale parachutes in supersonic flight has shown that the instability is driven by aerodynamic coupling of the parachute bow-shock and fore-body wake, and is dependent on Mach, Reynolds number, and proximity to and shape of the fore-body[6,7]. The shock-wake interactions affect the internal pressure distribution of the canopy, resulting in localized fabric collapse and re-inflation events (Fig. 1).

.

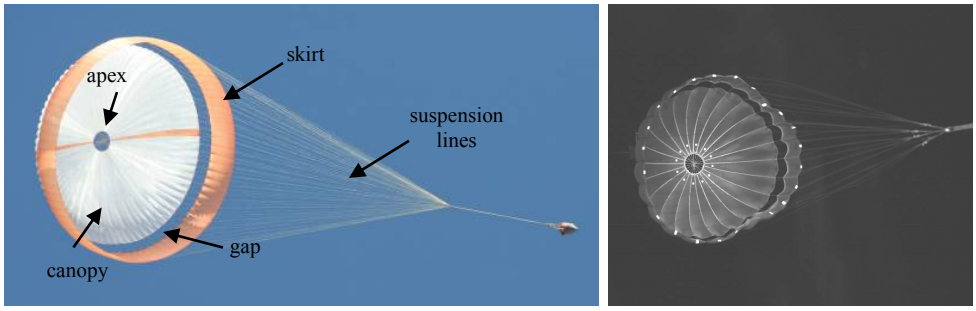

Fig. 1. (Left) Full-scale 21.5 m DGB parachute subsonic flight test on Earth. (Right) Subscale 0.8 m DGB.

II. Background

Supersonic use of aerodynamic decelerators for planetary entry was investigated extensively in 1960's and 1970's by the National Aeronautics and Space Administration (NASA) and is summarized in Table 1. The Planetary Entry Parachute Program (PEPP), Supersonic Planetary Entry Decelerator Program (SPED), and Supersonic High Altitude Parachute Experiment (SHAPE) conducted a series of Earth, high-altitude, supersonic flight tests for various parachute types (Ring Sail, Disk-Gap-Band, Cross) from 9 to 26 m in nominal diameter [8,9]. Following those efforts, in 1972, NASA conducted the Balloon Launched Decelerator Test (BLDT) program, intended to flight-qualify the parachute system for the upcoming Viking Lander mission to Mars. Through a series of four flight tests, the BLDT qualified a 16.1-m Disk-Gap-Band (DGB) parachute for use up to Mach 2.2 and 700 Pa [10,5]. In 1976, two Viking Landers, launched one month apart, were sent to Mars and successfully deployed their parachutes at Mach 1.1. They deployed at a lower Mach than the qualification limit, primarily due to a lack of knowledge of the Martian atmosphere. Twenty years passed before "supersonic" planetary-entry parachutes were used again. In 1997, the Mars Pathfinder mission successfully deployed a 12.7-m DGB parachute at Mach 1.7. In 2004, the two Mars Exploration Rover spacecraft deployed 14.1 m DGB parachutes at Mach 1.8 and 1.9 respectively. In 2004, the Huygen's Probe deployed a staged DGB parachute system at Mach 1.5 (2.6-m pilot, 8.3-m main, 3-m drogue) for its descent through Titan's atmosphere. In 2008, the Mars Phoenix Scout mission deployed an 11.7-m DGB parachute at Mach 1.9. All of these parachute flights were successful and employed a deployment Mach number and nominal diameter within the BLDT heritage qualification[11].

Table 1. Parachute parameters explored by the PEPP, SHAPE, SPED, and Viking BLDT program.

Parameter	Range Explored
d/D_o	0.2 - 0.3
x/d	4 - 10
Mach	0.5 to 3.0
Re	$10^5 - 10^6$
Q (Pa)	300-1000
C_D	0.3-0.7

In 2012, the Mars Science Laboratory (MSL) mission will deploy a 21.5-m DGB parachute at up to Mach 2.3 and 750 Pa at an altitude of 10km on Mars. These deployment conditions are just beyond the existing Viking qualification limit. In the absence of a full-scale supersonic test, an analytical understanding of the scale and Mach dependent, aero-structural response of the parachute is needed for its qualification. A two year research program was conducted to provide the needed physical insight into the scale, material, structural, and aero-elastic dependence of parachute operation in the supersonic regime[12]. A 2.1% of full-scale rigid parachute and 4% of full scale flexible parachute were tested in supersonic wind tunnels to determine the fluid structure interaction of the parachute with the 70-deg sphere cone entry vehicle wake. Details on the experimental techniques and computational developments can be found in references 13,14, and 15. The findings of that program will be presented in this paper in terms of Mach number, Reynolds number, geometric, and structural dependencies of DGB parachute operation in the supersonic regime.

III. Results and Findings

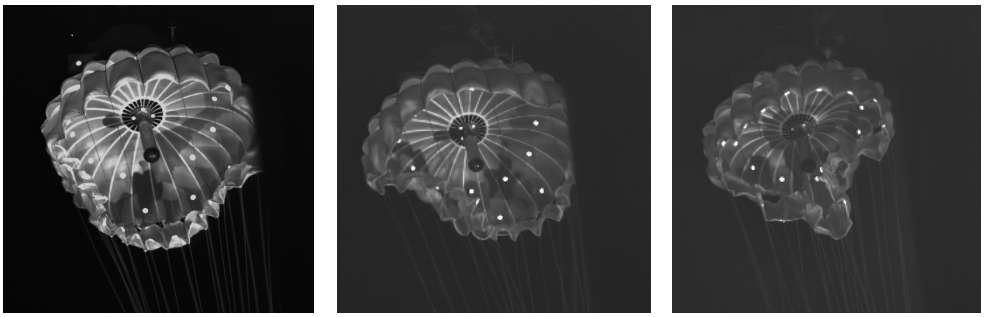

Fig. 2. Fig. 2. Images of the supersonic instability known as "area oscillations" (from left to right) at Mach 2.0, 2.2, and 2.5 for a 0.8-m DGB parachute [21].

Supersonic parachute aerodynamics were first investigated with subscale wind tunnel tests of ribbon parachutes from Mach 1.5 to 3 2. These studies revealed lateral and inflation instabilities as a function of Mach number and canopy porosity. The implications of these instabilities became obvious following the supersonic flight tests of the PEPP, SHAPE, SPED, and Viking BLDT programs. These flight tests revealed a supersonic breathing phenomenon that manifested at Mach numbers above 1.5 for parachutes flown in the wake of a "bluff body entry-vehicle. The instability, referred to as "area oscillations", is characterized by periodic collapse and re-inflation events that result in dynamic loading, projected area variation, and, in some cases parachute structural damage or failure (Fig. 2). The test programs of this era explored a large range of geometric and aerodynamic parameters, as summarized in Table 1. But a definitive aerodynamic basis of the area oscillation was never ascertained. This was largely due to the high frequency nature of the event and limited high-speed diagnostics and computational fluid dynamic capabilities at the time.

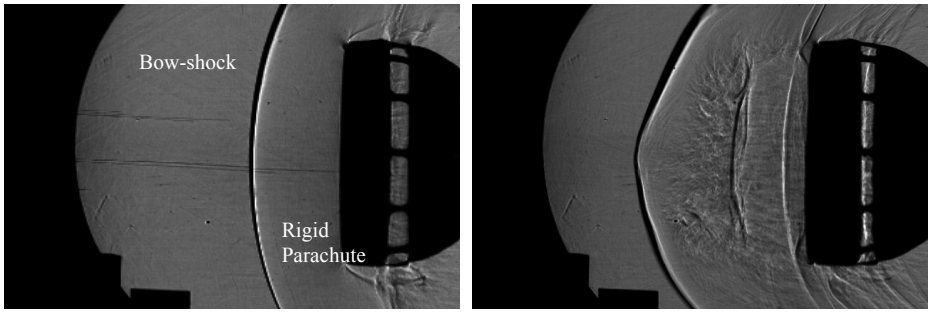

Fig. 3. Shadowgraph images comparing the effect of the entry-vehicle wake on the bow-shock just upstream of a 0.5-m rigid parachute at Mach 2.0. The left image has no entry vehicle. In the right image a 70-deg sphere-cone is located 10 entry-vehicle diameters upstream of the parachute 7. The flow direction is from left to right.

Recent experimental and computational studies, conducted in support of the next generation of Mars planetary-entry missions, have explored the aerodynamics of parachutes in supersonic flow. Subscale rigid and flexible DGB parachute experiments have revealed that the supersonic instability is the result of the fluid structure interaction of the coupling of the entry-vehicle wake to parachute bow-shock[13,14]. The momentum deficit of the subsonic wake causes the parachute's bow-shock to change in shape, move forward, and reduce mass flow into the canopy. During this time the canopy depressurizes and partially collapses, disrupting the primary bow-shock ahead of the canopy. The canopy then re-pressurizes and the bow shock is re-established. This process repeats cyclically at a frequency on the order of the acoustic frequency. A direct comparision of the flow-field of a rigid parachute with and without an entry-vehicle wake is shown in Fig. 3. In the absence of an upstream payload-wake, the bow-shock, pressure distribution inside of the canopy, and drag force are essentially constant. When a the entry-vehicle is inserted into the flow-field, the unsteadiness generated by the wake interaction is obvious (right hand image). In this case the bow shock oscillates and changes shape and the RMS drag is up to 50% of mean value. For the flexible parachute with an entry-vehicle, the flow-field is similar. A high-speed shadowgraph sequence of a flexible 0.8-m DGB parachute at Mach 2.0 is shown in Fig. 4. The oscillatory motion of the bow shock is clear. Also evident are shocks generated by the suspension lines (section 3.G).

Computational fluid dynamics simulations in conjunction with particle image velocity (PIV) measurements were also conducted to quantify the aerodynamic environment. Both data sets indicate the wake is time varying and highly unsteady [6,15]. A sample PIV measurement of the bow-shock wake coupling is shown in Fig. 5.

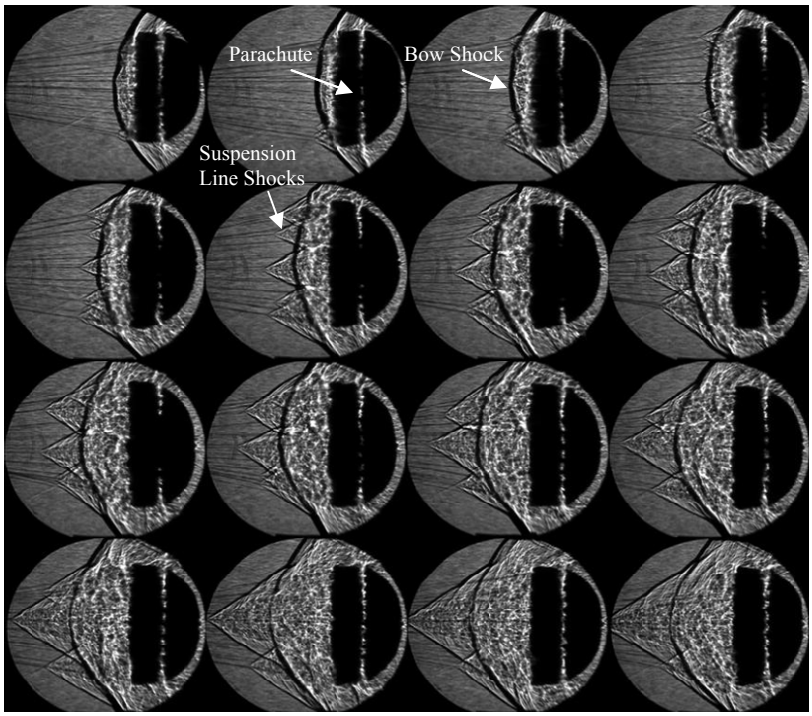

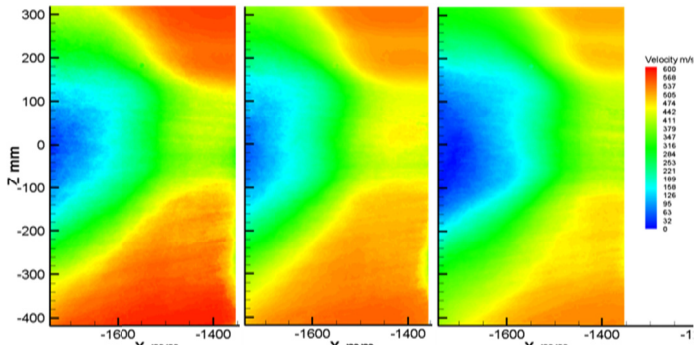

· **a**

A. Fabric Dynamics

In supersonic flight, the parachute fabric dynamics are primarily characterized by a high frequency flutter of the skirt. The area oscillation event occurs following the disruption of the bow-shock and subsequent depressurization of the canopy. During the event the skirt begins to in-fold and the canopy partically collapses, as shown in Fig. 2. The canopy breathing process results in large projected area variations, as low as 37% of the maximum achieveable area, as shown in Fig. 6. This coincides with highly unsteady drag performance, as will be discussed later. The frequency and severity of the parachute fabric dynamics increases with Mach and Reynold's number, consistent with wake-bow-shock coupling. The area oscillation frequency range is from $50/D_o$ to $70/D_o$ Hz (where

D_o is in [m]) from Mach of 2 to 2.5, as measured in both subscale wind-tunnel tests (D_o=0.8-m)and the full-scale Viking BLDT (D_o=16 m) [14]. The phenomenon is therefore absolute-scale independent. Another interesting feature of area oscillation is that its onset appears to be random. However, once established, each event is followed by 3 to 5 subsequent collapse and re-inflation events with a regular period. This is consistent with the randomess of the turbulent wake vortex shedding [16].

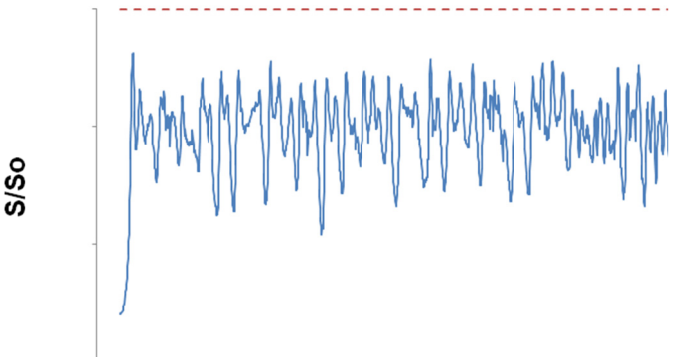

Mach
s the

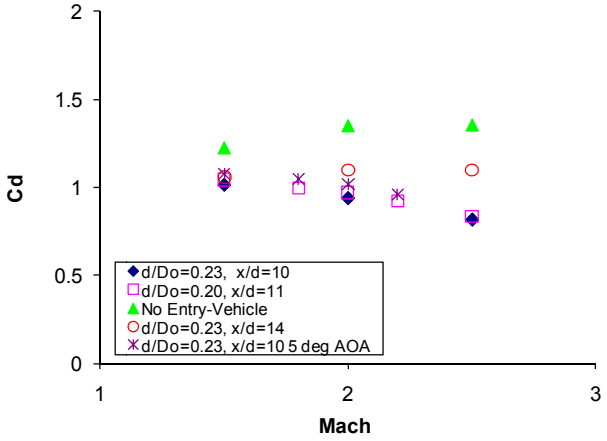

iations
ıgupta
l0⁶.

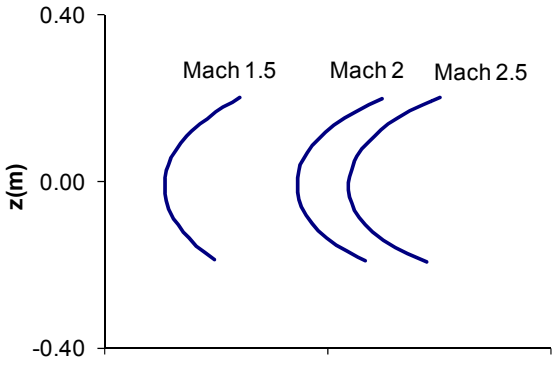

in the
2.5 and

B. Mach Dependence

Mach dependence in parachute performance has been observed by many researchers in wind tunnel and flight test programs [17,4,14,18]. From Mach 1.2 to 1.8 the drag coefficient tends to incease. However, from Mach 1.8 and higher, the drag coefficent decreases. To understand the aerodynamics of this phenomenon, a rigid parachute was placed in a wind tunnel, with and without a payload wake (Fig. 3). The drag coefficent as a function of Mach number is shown in Fig. 7. Figure 8 shows the corresponding bow shock stand-off distance and shape (for the "no entry-vehicle" case). In the parachute alone configuration, the reduction in drag effciency with Mach number is a result of the coupling of the parachute bow-shock to the free stream flow and resultant flow separation. For cases with an entry-vehicle wake, drag reduction is more evident, due to coupling of the subsonic wake to the bow-shock, and resultant canopy depressurization[7]. The flexible subscale parachute testing yielded similar results. Parachute drag efficiency reduces with increasing Mach number. Similaraly, fabric dynamics, dynamic loading, and canopy dynamics increase with Mach number. This is correlated with a more chaotic bowshock oscillation and more turbulent wake contribution to the bow-shock coupling[14].

C. Reynolds Number and Dynamic Pressure

The turbulent energy of the entry-vehicle wake is a major driver in the supersonic fluid structure interaction of the parachute. Reynolds number is the measure of turbulent energy, and typically varies from 105 to 106 for supersonic planetary entry applications. Reynolds number variation is easily achieved in the closed-loop wind tunnel by varying the static pressure or density, for the same Mach number (nozzle) setting[14]. The wake velocity structure was measured with PIV[15]. The axial wake structure from an *x/d* of 8 to 10 can be seen in Figures 9. The velocity contours indicate the radial extent of the wake deficit region, at the inlet to the parachute. Axial wake structure can be seen in the PIV measurement, as well. The higher

Reynolds number environment exhibited more severe area oscillations, including increased projected area variation, dynamic lateral motion (trim angle), and RMS drag.

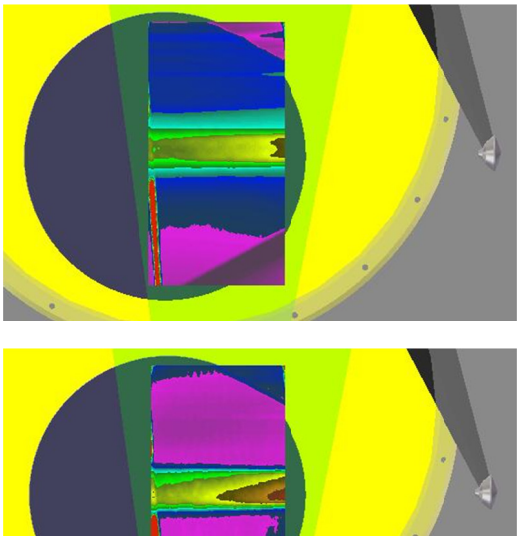

bottom)
-vehicle

D. Geometry Dependence

The shape, scale, proximity, and angle of attack of the parachute and bluff body entry-vehicle affect parachute performance. The ratio of parachute nominal diameter to entry-vehicle diameter (d/D_o) is a measure of the contribution of the wake to the fluid structure interaction. The non-dimensional trailing distance (x/d) is defined as the axial distance between the parachute leading-edge and entry-vehicle maximum diameter. Non-zero capsule angle of attack and parachute trim angle (relative to the velocity vector) results in an asymmetric flow into the canopy mouth.

Wind tunnel tests with a rigid parachute in the wake of a bluff body explored the geometric dependencies of the parachute entry-vehicle fluid structure interaction[19]. Figure 10 details the drag coefficient variation versus Mach number for a variety of geometric parameters. Consistent with the finding that the entry-vehicle wake is the source of the flow field unsteadiness, an increase in d/D_o tends to reduce the flow field unsteadiness. Similarly, increasing trailing distance reduces the coupling of the wake to bow-shock and the drag coefficient is higher. At an x/d=14, the C_D with Mach curve begins to resemble that of the canopy alone configuration. Therefore, in the limit of $x/d \rightarrow \infty$ or $d/D_o \rightarrow 0$, the effective entry-vehicle diameter approaches zero, i.e. the flow-field approaches that of the parachute without an upstream wake contribution.

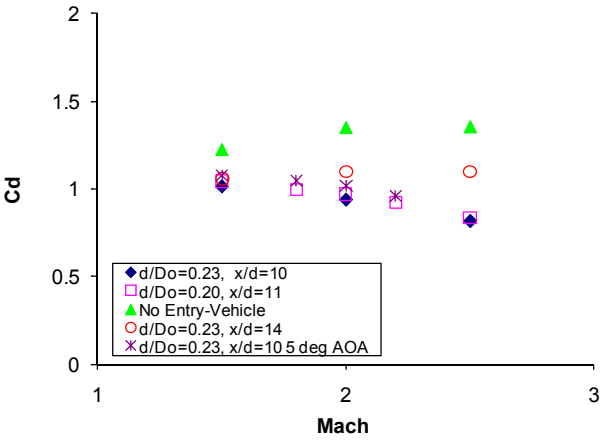

variations

In general, the flow physics associated with a range of parachute geometric parameters is continuous and dependent on the degree of coupling between the wake and parachute bow-shock. Selection of an appropriate trailing distance can reduce coupling, but it must be traded with an orderly deployment process, parachute inflation time, and multi-body dynamics considerations.

E. Structural Implications

The supersonic regime has a direct impact on parachute loading and consequently the design and material selection of the canopy. The unsteady aerodynamic environment leads to an asymmetric pressure distribution, collapse and wrinkling of the fabric, and dynamic drag. The area oscillation collapse and re-inflation process leads to self abrasion, material fatigue, a high rate of strain, and dynamics overshoots of up to 200% of the mean drag force.

The average axial force or drag (D) experienced by a parachute is a function of the dynamic pressure (Q), parachute area (A), and drag coefficient (C_D)[3].

$$D_{avg} = QC_D A \qquad (1)$$

In subsonic applications parachute loading is dominated by the initial inflation load. Dynamic and asymmetric loading are dissipated by the time the canopy is fully inflated. Subsequent loading is at a lower level due to the

deceleration of the parachute and payload with time and altitude. This is defined by the ratio of the initial inflation load to average load (C_x)[20].

$$C_{x,i} = \frac{D_i}{D_{avg}} \tag{2}$$

In supersonic applications the drag force on the canopy is highly unsteady and cyclical as shown in Fig. 11. This is consistent with the canopy pressurization/depressurization process and resulting fabric dynamics or canopy breathing. A fully inflated state may not be attained prior to the onset of area oscillations. Therefore, the initial inflation load does not necessarily represent the peak load. A maximum load factor is therefore required to define the supersonic loading environment ($C_{x,max}$).

$$C_{x,\max} = \frac{D_{\max}}{D_{avg}} \tag{3}$$

The supersonic load factor was determined experimentally via wind tunnel test environment for Mars representative conditions7. The load factor from Mach 2 to 2.5 is shown in Fig. 12. The maximum load is greater than two times the average drag load due to the highly unsteady aerodynamic environment. $C_{x,max}$ increases with Mach number whereas $C_{x,i}$ has a maximum at Mach 2.2 Therefore, increased canopy breathing with Mach number results in the potential for lower initial load.

Knacke developed a set of factors to account for load asymmetry, dynamic loading, abrasion, and fatigue. Traditional subsonic parachute factors will inadequately size the parachute for peak load in a supersonic fluid structure interaction environment. The asymmetry and dynamic loading due to the non-uniform pressure distribution and highly unsteady flow-field must be accounted for. Similarly, fatigue and abrasion are exacerbated due to the parachute breathing. A comparison of newly derived supersonic and existing subsonic load and loss factors is shown in Table 13.

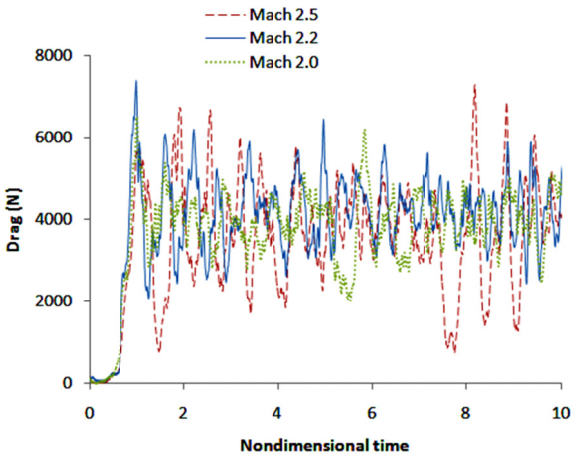

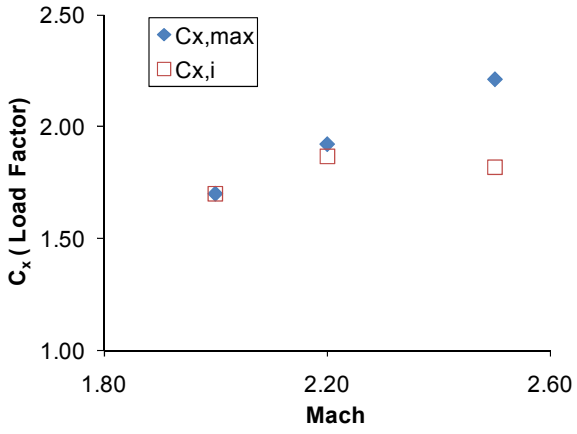

nts at [14].

1S

Table 1. Comparison of subsonic and supersonic load and loss factors 3.

Aerodynamic Regime	Load Factors		Loss Factors	
	Unsymmetric Load	Dynamic Load (C_x)	Abrasion	Fatigue
Subsonic	1.0-1.1	1-1.1	0.97-1.0	0.95-1.0
Supersonic	2.0-2.5	2.0-2.5	0.9	0.9

F. Parachute Performance

Parachute performance is typically gauged in terms of drag and stability. Measurements of parachute drag as a function of *Re* and Mach number are shown in Fig. 13. The test parachute was flown in the wake of an entry vehicle with a d/D_o of 0.21 and x/d of 10 (Sengupta et. al. 2009[a]). Drag coefficient reduces with increasing Mach number, which is consistent with bluff-body flows. Drag coefficient does not appear to vary with Reynolds number, however, in the range of 10^5 to 10^6. This is a key finding as Reynolds number variation was achieved via dynamic pressure variation. Fabric porosity variation with dynamic pressure was previously thought to be the driver of the supersonic instability. This does not appear to be the case. As discussed earlier, the contribution of turbulence is due to the energy content of the wake and resultant unsteadiness of the flow field.

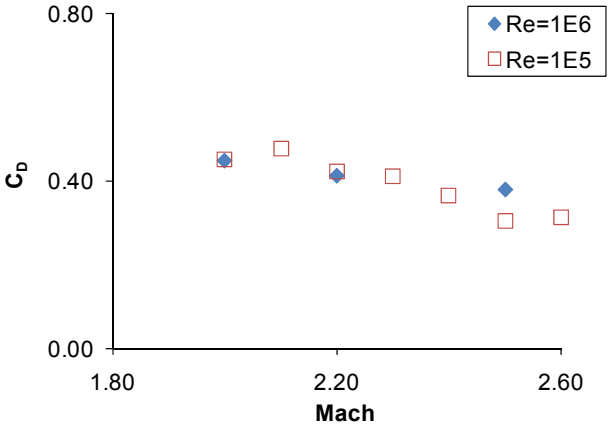

Fig. 13. Parachute DGB drag performance as a function of Mach and Reynolds number for a d/D_o=0.21, and x/d=10 [14].

Parachute stability is characterized by the trim angle it experiences during flight. The wind tunnel testing of subscale DGB parachutes indicates a trim angle excursion of 4 to 8 degrees from Mach 2 to 2.5. This range of variation is similar to that of the subsonic variation, albeit at a high coning frequency.

G. Suspension Line Interaction

The parachute suspension-lines can generate their own shocks, generating large density disturbances, as can be seen in shadowgraph sequence of Fig. 14. Correlation of high-speed video and shadowgraph data reveal that suspension-line shocks are generated when the canopy starts to collapse. The suspension-line shocks creep up the lines until they intersect with the primary bow-shock. The aerodynamic interaction with bow-shock tends to exacerbate the bow-shock dynamics, contributing to the bow-shock disruption and area oscillation. The subscale parachutes used in the wind tunnel test program had a line thickness to diameter ratio similar to that of the Viking BLDT era parachutes. However, the Viking BLDT parachutes have approximately six times thicker (Dacron) suspension-lines as compared to modern day Kevlar line parachutes of the same size (Dickenson et al., 1972). This is a critical finding in that the thickness of the suspension-lines may play a role in the severity of the supersonic instability, with modern day parachutes having a reduced suspension-line interaction and potentially less severe dynamic loading.

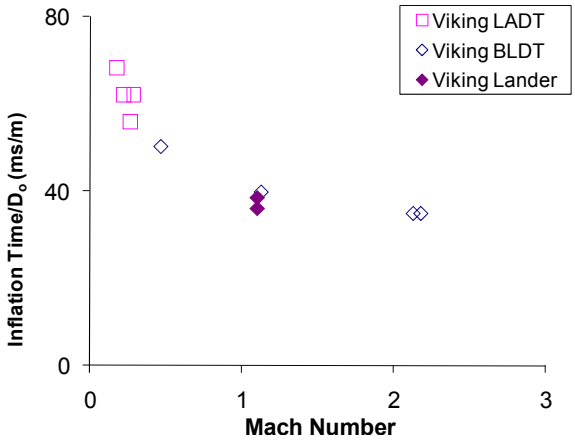

Fig. 14. Comparison of subsonic to supersonic DGB parachute inflation times for a d/D_o=0.22, and x/d=8.5 [10].

H. Inflation Time

Parachute inflation time is a commonly used performance metric. The inflation time (t_i) is a function of the free-stream velocity (v), diameter of the parachute (D_o), and parachute type (n). *Knacke* proposed the following relation for subsonic parachutes3.

$$t_i = \frac{nD_o}{v} \tag{3}$$

A review of existing data for both supersonic and subsonic deployments DGB parachutes confirms this linear relationship over the subsonic *and* supersonic regimes, as shown in Fig. 15 for the 16.1-m Viking DGB parachute, shown in units of t_i/D_o.

High-speed video recorded during the subscale supersonic wind tunnel testing has provided qualitative insight into the supersonic inflation process, as shown in Fig. 15. The inflation time, t_i/D_o ranged from 10 to 20 ms/m from Mach 2 to 2.5 respectively[14,21]. The parachute inflates from the skirt exhibiting a multi-gore in-fold that unfurls prior to full inflation. The time scale of the supersonic inflation is such that flag drag and flapping dynamics are not present. The inflation dynamics were similar and repeatable, in terms of initial presentation and evolution of the canopy from Mach 2 to 2.5. Shadowgraph data were also recorded during the inflation process. The shock structure changed from attached to detached as the canopy inflated. During this transition shock disruption can occur, but does not result in an area oscillation. It should also be noted that the partially inflated canopy resembles that of an area oscillation event, suggesting that inflation recovery is not an issue for the supersonic instability.

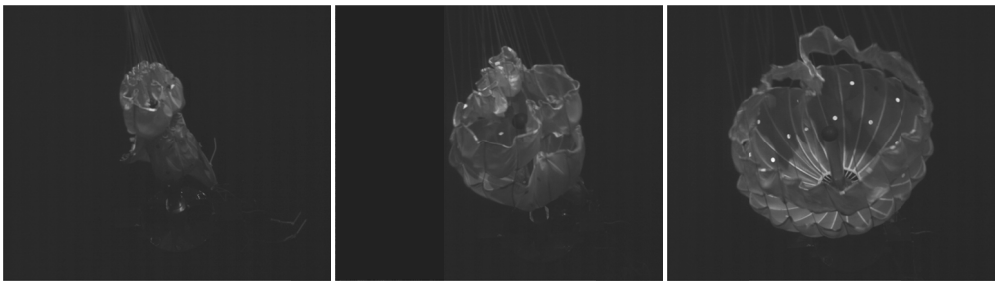

IV. Verification and Validation

Deployment conditions for planetary-entry parachutes are often characterized by low atmospheric densities at supersonic speeds. As such, the "test as you fly" methodology for qualification is expensive and often in the literal sense impossible to achieve. For example, although the Viking BLDT program deployed at the Mach and dynamic pressure of a Mars parachute deployment, the acceleration due to gravity and ratio of specific heats cannot be achieved on Earth, resulting in differences in shock angle, Reynolds number, and ballistic coefficient (or rate of descent). An analytical understanding of the physics of the parachute operation is required to translate between Earth-based tests and the actual flight environment. Similarly, physics based non-dimensionalization of key geometric, aerodynamic, and structural parameters enables subscale testing and interpolation/extrapolation of existing heritage datasets. In addition, as will be discussed in the next section, computational tools can be used in the detailed design of parachute systems for prediction of aerodynamic phenomena, fabric stresses, and multi-body dynamics [12].

Decelerators, in general, can be qualified based on five different operational regimes: deployment from the entry-vehicle, inflation to the fully open state, structural integrity due to initial inflation, and subsequent loading, supersonic flight, and subsonic flight. Each of these aspects can be verified and validated independently by a combination of ground tests in a relevant environment in conjunction with analytical methods. This approach was used successfully by the Mars Pathfinder, Mars Exploration Rover, and Phoenix parachute systems that all performed nominally in their supersonic descent through the Martian atmosphere. A detailed discussion of this verification and validation approach can be found in reference 18.

The aspect of supersonic qualification can be addressed by subscale test and computational simulation validation. Subscale validation tests can be designed and executed to explore aerodynamic, geometric, and structural dependencies of the parachute in supersonic flight. In addition, bench-mark experiments can be used to explore individual elements of the program (entry-vehicle, parachute alone, coupled flow-field). Use of non-intrusive, spatially and temporally resolved diagnostics can provide high fidelity datasets from each experiment to validate the computational tool to a new level of fidelity. An example of this is shown in Fig. 16 for a parachute system.

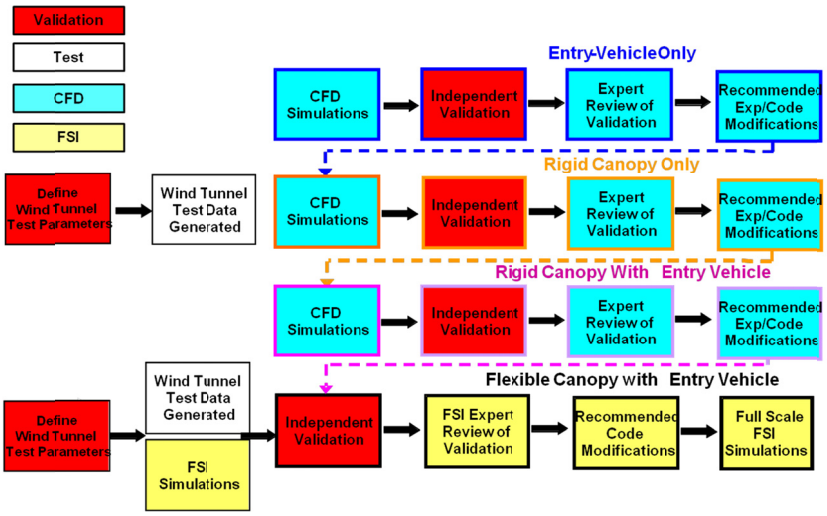

V. Future Work

The supersonic fluid structure interaction problem is far from solved. In fact it is an issue for all aerodynamic decelerators including parachutes, trailing ballutes, and attached inflatable decelerators for supersonic and hypersonic entry applications. Current work in this area is focused on the development and validation of computational fluid dynamics (CFD) and finite element modelling (FEM) simulation capabilities. Validated computational tools minimize the need for prohibitively expensive test programs and can be used in the design and material selection of decelerators. Due to the complexity of the flow-field, large eddy simulation capability, shock capturing, and three-dimensional high density computational grids are needed to resolve the turbulent wake and bow-shock interaction, accurately. Similarly, solid dynamic solvers must have the ability to model the parachute membrane wrinkling and self-contact. A Fluid Structure Interaction (FSI) simulation capability is the coupling of CFD and FEM simulations, where predicted aerodynamic forces deform the parachute membrane and vice versa. FSI is needed to accurately predict the stress distribution and fabric dynamic response to the aerodynamic environment. A key challenge associated with FSI tool development is the ability to restructure the fluid grid in time as the parachute translates and collapses in response to the aerodynamic forces. Several FSI codes are under development in the academic community with preliminary validation showing promising results [13,6,22].

Near term supersonic decelerator use includes the upcoming NASA Mars Science Laboratory mission (2012), the European Space Agency's Exomars mission (2016), and supersonic inflatable decelerator flight tests like NASA's Inflatable Re-Entry Vehicle Experiment (IRVE)[23].

VI. Conclusion

Supersonic use of aerodynamic decelerators has been limited due to concern of the instability known as area oscillations. Through a series of subscale wind tunnel tests with non-intrusive diagnostic techniques, the fluid structure interaction environment of the parachute and entry-vehicle wake was characterized and quantified from Mach 1.5 to 2.5. In the absence of a turbulent wake, the parachute supersonic flow-field is relatively steady with little dynamic loading. However, when a bluff body entry-vehicle is inserted upstream of the parachute, the flow

field becomes unsteady and the parachute responds with the area oscillation process. The mechanism discovered is the turbulent wake coupling to the parachute's bow-shock causing it to change shape and standoff distance, resulting in depressurization of the canopy and resultant partial collapse. Following disruption of the bow shock the canopy re-pressurizes and the process repeats itself in a cyclical manner. A critical finding is the effect of suspension line shocks on the bow-shock disruption, adding to the severity and frequency of the collapse events and dynamic loading. Mach and Reynolds dependence of the flow field was also explored over the range of Mach 2 to 2.5. Flow-field unsteadiness is directly related to the energy content of the wake and proximity to the canopy mouth. Measurements of parachute performance were also obtained. Drag efficiency decreases monotonically with Mach number but does not appear to depend on Reynolds number to first order. Dynamic loading, lateral motion, and fabric dynamics of the parachute increase with Mach and Reynolds number. These factors play a critical role in the design and test of parachutes for supersonic use. The parachute's response to the aerodynamic environment is primarily based on its coupling to entry-vehicle wake. The rigid parachute experiment verified that the entry-vehicle wake is the source of the supersonic instability. Values derived from the subscale wind tunnel environment also compare surprisingly well with the Viking BLDT flight test data. Therefore, non-dimensional aerodynamic and geometric scaling parameters are valuable metrics in understanding the physics of supersonic parachute operation.

Acknowledgments

The authors would like to acknowledge the support of Leslie Hall from the Georgia Institute of Technology, Mark Wernet, James Roeder and Rick Kelsch from NASA Glenn Research Center, and Al Witkowski from Pioneer Aerospace. This work was carried out at the Jet Propulsion Laboratory, California Institute of Technology, under a contract with the National Aeronautics and Space Administration.

References

[1] Murrow H. & Eckstrom C. (1970). Low and High Altitude Tests of Parachutes Designed for Use in Low Density Atmospheres, Proceedings of the AIAA 3rd Decelerator Systems Conference, Dayton, Ohio, September 1970, AIAA, Washington D.C.

[2] Maynard, J., (1960). Aerodynamics of Decelerators at Supersonic Speeds, Proceedings of the Recovery of Space Vehicles Symposium Los Angeles, California, Institute of Aeronautical Sciences, Washington D.C. (1960).

[3] Knacke, T., (1992). *Parachute Recovery Systems Design Manual*, Para Publishing, ISBN 0-0915516-85-3, Santa Barbara, California.

[4] Reichenau., D.E. (1972). Aerodynamic Characteristics of Disk-Gap-Band Parachutes in the Wake of Viking Entry Forebodies at Mach Numbers from 0.2 to 2.6, Arnold AFB, AEDC-TR-72-78, Tennessee.

[5] Dickenson, D. et al. (1972). Balloon Launched Decelerator Test Post-Flight Test Report BLDT Vehicle AV1, Martin Marrieta Corp., TR-3720289, Denver, Colorado.

[6] Barnhardt, M.; Drayna, T.; Nompelis, I.; Candler, G.; & Garrard, W. (2007). Detached Eddy Simulations of the MSL Parachute at Supersonic Conditions, Proceedings of the 19th AIAA Aerodynamic Decelerator Systems Technology Conference, Williamsburg, Virginia, May 2007, AIAA, Washington, D.C.

[7] Sengupta, A.; Steltzner, A.; Comeaux, K.; Candler, G.; Pantano, C.; Bell, J.; Heineck, J., & Shairer, E., "Results from the Mars Science Laboratory Parachute Decelerator System Supersonic Qualification Program," Proceedings of the IEEE Aerospace Conference, pp. 1 – 15, Big Sky, Montana, March 2008, IEEE, Washington D.C.

[8] Murrow, H. & Mcfall, J. (1969). Some Test Results from the NASA Planetary Entry Parachute Program. J. Spacecraft, Vol. 6, No. 5, (May 1969) pp. 621-623.

[9] Murrow, H. & Mcfall, J. (1968). Summary of Experimental Results Obtained from the NASA Planetary Entry Parachute Program Summary," Proceedings of the AIAA 2nd Decelerator Systems Technology Conference, El Centro, California, September 1968, AIAA, Washington, D.C.

[10] Moog, R.D. & Michel, F.C (1973). Balloon Launched Viking Decelerator Test Program Summary Report, Martin Marrieta Corp., TR-372039, Denver, Colorado.

[11] Cruz, J. & Lingard, S. (2006). Aerodynamic Decelerators for Planetary Exploration: Past, Present, and Future, Proceedings of the AIAA Guidance, Navigation, and Control Conference and Exhibit, Keystone, Colorado, August 2006, AIAA, Washington D.C.

[12] Sengupta, A.; Steltzner, A.; Witkowski, A.; Candler, G.; Pantano, C. (2009). Findings from the Supersonic Qualification Program of the Mars Science Laboratory Parachute System, Proceedings of the 20th AIAA

Aerodynamics Decelerator Systems Technology Conference, Seattle, Washington, May 2009, AIAA, Washington D.C.
[13] Sengupta, A.; Steltzner; A., Comeaux, K.; Candler, G.; Pantano, C.; & Bell, J. (2007). Supersonic Delta Qualification by Analysis Program for the Mars Science Laboratory Parachute Decelerator System, Proceedings of the 19th AIAA Aerodynamic Decelerator Systems Technology Conference, Williamsburg, Virginia, May, 2007, AIAA.
[14] Sengupta, A.; Wernet, M.; Roeder, J.; Kelsch, R.; Witkowski, A.; & Jones, T. (2009) Supersonic Testing of 0.8 m Disk Gap Band Parachutes in the Wake of a 70 deg Sphere Cone Entry Vehicle, Proceedings of the 20th AIAA Aerodynamics Decelerator Systems Technology Conference, Seattle, Wasington, May 2009, AIAA, Washington D.C.
[15] Wernet, M.; Locke, R.; Wroblewski, A.; & Sengupta, A. (2009). Application of Stereo PIV on a Supersonic Parachute Model, Proceedings of the 47th AIAA Aerospace Sciences Conference, Orlando, Florida, Jan 2009, AIAA, Washington D.C.
[16] Pope, S. (2000). Turbulent Flows, Cambridge University Press, 0521598869, New York.
[17] Jaremenko, I.; Steinberg, S.; & Faye-Petersen, R. (1971). Scale Model Test Results of the Viking Parachute System at Mach Numbers from 0.1 Through 2.6, NASA, TR-3720181.
[18] Sengupta, A.; Steltzner; A., Witkowski; A.; & Rowan, J. (2007). An Overview of the Mars Science Laboratory Parachute Decelerator System, Proceedings of the IEEE Aerospace Conference, Big Sky, Montana, pp. 1-8, March 2007, IEEE, Washington, D.C.
[19] Sengupta, A.; Steltzner; A., Comeaux, K.; Candler, G.; Pantano, C.; & Bell, J. (2007). Supersonic Delta Qualification by Analysis Program for the Mars Science Laboratory Parachute Decelerator System, Proceedings of the 19th AIAA Aerodynamic Decelerator Systems Technology Conference, Williamsburg, Virginia, May, 2007, AIAA.
[20] Cruz, J., Kandis; M., & Witkowski, A. (2005). Opening Loads Analyses for Various Disk-Gap-Band Parachutes, Proceedings of the 17th AIAA Aerodynamic Decelerator Systems Technology Conference, Monterey, California, May 2003, AIAA, Washington D.C.
[21] Sengupta, A.; Wernet, M.; Roeder, J.; Kelsch, R.; Witkowski, A.; & Kandis, M. (2008). Supersonic Disk Gap Band Parachute Performance in the Wake of a Viking-Type Entry Vehicle from Mach 2 to 2.5, Proceedings of the 26th AIAA Applied Aerodynamics Conference, Honolulu, Hawaii, August 2008, AIAA, Washington D.C.
[22] Karagiozis, K., Fehmi, C., Kamakoti, R., Pantano, C., Gidzak,V., Nompelis, I., Stein, K., & Candler, G. (2007). Computational Fluid-Structure Interaction Methods for Simulation of Inflatable Aerodynamic Decelerators, Proceedings of the 19th AIAA Aerodynamic Decelerator Systems Technology Conference, Williamsburg, Virginia, May 2007, AIAA, Washington, D.C.
[23] R. Dillman et. al.,"Flight Performance of the Inflatable Re-entry Vehicle experiment II," Interplanetary Probe Workshop, Barcelona, Spain, June 2010.